Pergamon

Int. J. Heat Mass Transfer. Vol. 39, No. 14, pp. 2957–2968, 1996

0017-9310/96 $15.00 + 0.00

0017-9310(95)00363-0

Polymer melt flow and gas penetration in gas-assisted injection molding of a thin part with gas channel design

SHIA CHUNG CHEN, KUO FU HSU and KE SHENG HSU

Mechanical Engineering Department, Chung Yuan University, Chung-Li, Taiwan 32023, Republic of China

(*Received* 26 *August* 1994 *and in final form* 25 *September* 1995)

Abstract—Numerical simulations and experimental studies concerning gas and melt flow during gas-assisted injection molding of a thin, angle bracket part with gas channel design were conducted. Distribution of skin melt thickness along the gas flow direction was measured. Melt and gas flow within the gas channel of a quadrantal cross-section is approximated by a model which uses a circular pipe of equivalent hydraulic diameter superimposed on the thin part. An algorithm based on a control-volume/finite-element method combined with a particle-tracing scheme suitable for two-component flow front advancements is utilized and numerically implemented to predict both melt and gas front advancements during a molding process. Simulated results on the distribution of gas penetration show reasonably good coincidence with experimental observations. Copyright © 1996 Elsevier Science Ltd.

1. INTRODUCTION

Gas-assisted injection molding is one of the innovative multi-component injection molding processes recently developed. In the gas-assisted injection molding, the mold cavity is partially filled with polymer melt followed by the injection of inert gas into the core of the polymer melt [1–4]. A schematic diagram of the gas-assisted injection molding is illustrated in Fig. 1. Compared with a conventional injection molding, the required injection pressure is greatly reduced. As a result, residual stress and warpage within the molded part can be minimized and part quality can be improved. Despite the advantages associated with the process, the molding window and process control become more critical and difficult since additional processing parameters are involved. These new gas-related processing parameters include the amount of melt injection, gas pressure, delay time of gas injection and gas injection time, etc. During the gas injection stage, gas usually takes the path of least resistance to catch up with the melt front. In order to guide the gas flow to the desired location and/or the designed distribution, part design using thick ribs as gas channels also becomes a dominant factor for the successful application of the process. In general, due to the complexity of gas channel design, the process control as well as the different flow characteristics between gas and melt, computer simulation is expected to become an important and a required tool to help in both part design and process evaluation in the coming age.

For nearly a decade, a simulation model based on a Hele–Shaw type of flow has been developed to describe the polymer melt flow in thin cavities during conventional injection moldings. Two typical types of control volume/finite element formulations were employed [5, 6]. These simulations provide acceptable predictions from the engineering application point of view. Now, the existing models meet the new challenge and must be adapted to handle both gas and melt flows in the cavities of non-uniform thickness. Although a complete three-dimensional analysis may be the final solution, the computational cost is too expensive to be implemented at the present stage for an engineering design purpose. At the present stage, a numerical algorithm suitable for the simulation of both gas and melt front advancements, as well as the empirical model describing the melt thickness between the solidified melt and gas/melt interface (Fig. 2) as a function of processing parameters, material properties and/or flow geometry are both required for an accurate simulation of the gas-assisted injection molding process. For parts laid out with gas channels, which are usually of pipe-like flow leader, the flow algorithm should also be adjusted to describe these mixed one-dimensional and two-dimensional flow characteristics. In the present paper, we first utilize a circular pipe of equivalent hydraulic diameter and a superimposition approach [8] to represent the mixed one-dimensional and two-dimensional flow characteristics for melt and gas flow in the gas channel of non-circular cross-section. Such an analysis approach has been verified for melt flow in a thin cavity with a rib of semicircular cross-section reported recently [8]. Then an algorithm based on the control-volume/finite-element method combined with a particle-tracing scheme using dual filling parameter technique was developed to simulate both gas and polymer melt flow

NOMENCLATURE

B	viscosity constant, equation (13)
B_i	$=y_j-y_k$
b	half gap thickness
C_i	$=x_k-x_j$
C_P	specific heat of polymer melt
D_{ik}	influence coefficient, equation (14)
$\{G\}$	column matrix of equation (19)
$[K]$	coefficient matrix of equation (19)
k	thermal conductivity of polymer melt
L	length of runner element
n	viscosity constant, equation (12)
P	pressure
$\{P\}$	column matrix for pressure
Q	volumetric flow rate
q_i	net flow rate at node i, equation (14)
R	radius of runner
r	radial direction of pipe
S	fluidity, equations (6) and (11)
T	temperature
T_b	reference temperature, equation (13)
u	velocity in x-direction
$\bar{u}$	averaged velocity along z-direction for u
v	velocity in y-direction
$\bar{v}$	averaged velocity along z-direction for v
w	velocity in axial direction of runner
$\bar{w}$	averaged velocity along r-direction for w
x	planar direction
y	planar direction
z	gapwise direction of cavity or axial direction of runner.

Greek symbols

Δ	area of a triangular element
η	viscosity
η_0	viscosity constant, equation (12)
$\dot{\gamma}$	shear rate
ρ	density of polymer melt
τ^*	viscosity constant, equation (12).

Subscripts

i	designation of local node index in an element
j	designation of local node index in an element
k	designation of local node index in an element
gas	designation of gas-related parameter
melt	designation of melt-related parameter.

Superscripts

l	designation of lth adjacent element
l'	designation of l'th adjacent element.

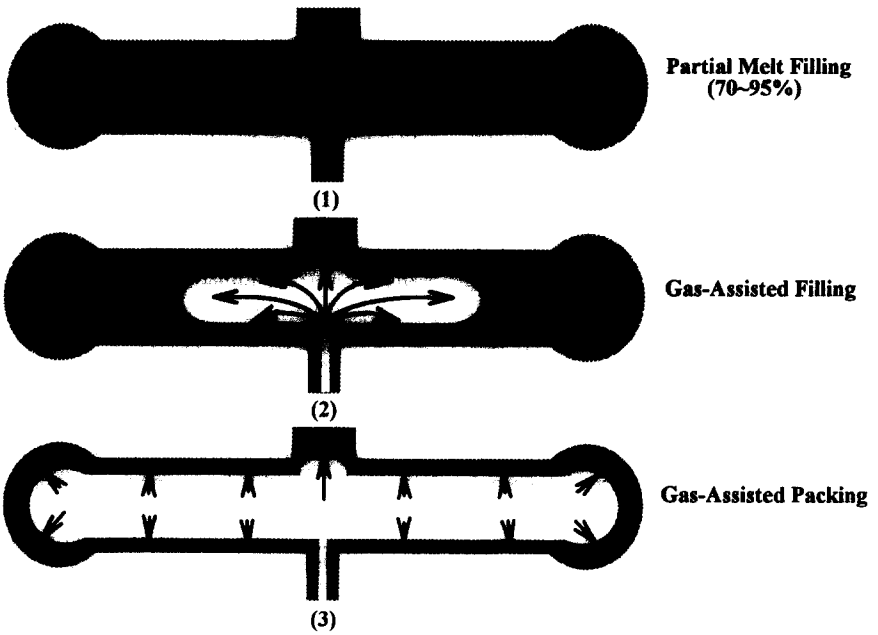

Fig. 1. Schematic of gas-assisted injection molding process.

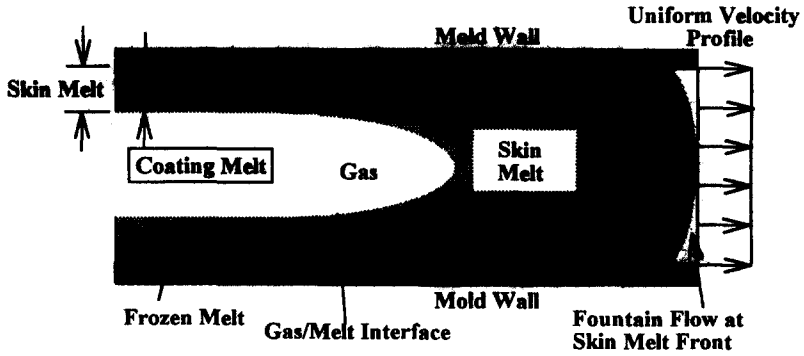

Fig. 2. Schematic view of gas penetration along gapwise direction.

during the filling process of gas-assisted injection molding. This particle-tracing scheme is modified from the algorithm concept successfully used for the calculation of skin and core melt front advancements during a coinjection molding process [9]. The present numerical algorithm and the associated simulations are also applied to a gas injection molded spiral tube of purely one-dimensional flow and tested for a thick hanger part under a planar flow condition, respectively. Verification of the predicted results by experiments shows positive confirmation. Finally, a thin angle bracket part laid out with a gas channel of quadrantal cross-section is gas-assisted injection molded. The coating melt thickness between solidified melt and gas was investigated and measured along the gas flow direction. Simulated results for the advancements of melt and gas front within the filling period are illustrated and discussed. The predicted distribution of gas penetration is compared with experimental observation.

2. MODELING AND FORMULATION

It has been generally accepted that the Hele–Shaw type of flow model provides a reasonably accurate description of polymer melt flow in a three-dimensional thin cavity. As a result, the relevant governing equations for the inelastic, non-Newtonian fluid flow under non-isothermal conditions are similar to those used in conventional injection molding [5, 7]

$$\frac{\partial P}{\partial x} = \frac{\partial}{\partial z}\left(\eta \frac{\partial u}{\partial z}\right) \tag{1}$$

$$\frac{\partial P}{\partial y} = \frac{\partial}{\partial z}\left(\eta \frac{\partial v}{\partial z}\right) \tag{2}$$

$$\frac{\partial}{\partial x}(b\bar{u}) + \frac{\partial}{\partial y}(b\bar{v}) = 0 \tag{3}$$

$$\rho C_P\left(\frac{\partial T}{\partial t} + u\frac{\partial T}{\partial x} + v\frac{\partial T}{\partial y}\right) = k\frac{\partial^2 T}{\partial z^2} + \eta\dot{\gamma}^2 \tag{4}$$

where P, T, u and v represent pressure, temperature and melt velocities in the x- and y-directions, respectively. b is the half thickness of mold cavity in a gapwise direction z, $\bar{u}$ and $\bar{v}$ are averaged velocities gapwisely for u and v, correspondingly. In addition, $\dot{\gamma}$, η, ρ, C_P and k are shear rate, viscosity, density, specific heat and thermal conductivity for the polymer melt.

Equations (1) and (2) can be integrated into equation (3) and become

$$\frac{\partial}{\partial x}\left(S\frac{\partial P}{\partial x}\right) + \frac{\partial}{\partial y}\left(S\frac{\partial P}{\partial y}\right) = 0 \tag{5}$$

with

$$S = \int_0^b \frac{z^2}{\eta}\,dz. \tag{6}$$

The governing equations for the one-dimensional melt flow in the delivery system (runner) can also be written in a similar way, but in cylindrical coordinate by

$$\frac{\partial}{\partial z}(\pi R^2 \bar{w}) = 0 \tag{7}$$

$$\frac{\partial P}{\partial z} = \frac{1}{r}\frac{\partial}{\partial r}\left[r\left(\eta\frac{\partial w}{\partial r}\right)\right] \tag{8}$$

$$\rho C_P\left(\frac{\partial T}{\partial t} + w\frac{\partial T}{\partial z}\right) = \left[\frac{1}{r}\frac{\partial}{\partial r}\left(rk\frac{\partial T}{\partial r}\right)\right] + \eta\left(\frac{\partial w}{\partial r}\right)^2 \tag{9}$$

where w is the velocity in the axial direction, z, r are the radial direction, $\bar{w}$ is the averaged velocity of w along radial direction and R is the radius of the runner.

Equations (7) and (8) can also be formulated into an integrated form described by

$$\frac{\partial}{\partial z}\left(\pi S\frac{\partial P}{\partial z}\right) = 0 \tag{10}$$

with

$$S = \int_0^R \frac{r^3}{2\eta}\,dr. \tag{11}$$

The non-Newtonian characteristics of polymer melt viscosity are described by a form of modified-Cross model with Arrhenius temperature dependence, that is,

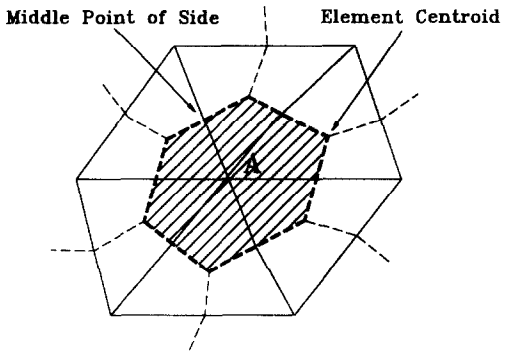

Fig. 3. Schematic of a control volume centered at node A. The control volume is constructed by connections of the centroids of all the adjacent finite elements around node A.

$$\eta(T,\dot{\gamma}) = \frac{\eta_0(T)}{1+(\eta_0\dot{\gamma}/\tau^*)^{1-n}} \tag{12}$$

with

$$\eta_0(T) = B\exp\left(\frac{T_b}{T}\right) \tag{13}$$

where T_b, B, η_0, τ^* and n are constants.

3. NUMERICAL ALGORITHM

3.1. *Algorithm for melt front advancement during melt injection*

Melt flow in conventionally injected molded thin cavities. In solving the pressure field during a melt injection period, equation (5) and equation (10) of the Laplacian form are discretized using the standard Galerkin finite element method [10]. The control volume formulation can also be employed directly to obtain the same discretized form [5, 7]. The net flow, $q_i^{(l)}$, that enters its control volume, centered at node A (Fig. 3), from an adjacent element l can be represented by

$$q_i^{(l)} = S^{(l)} \cdot \sum_{k=1}^{2\text{ or }3} \cdot D_{ik}^{(l)} \cdot P_k^{(l)} \tag{14}$$

where i is the local index for node A in element l and $i = 1$, 2, or 3 for triangular elements and $i = 1$ or 2 for rod-like elements. Subscript k denotes the local node index in element l and $D_{ik}^{(l)}$ is the influence coefficient of the nodal pressure to the net flow in element l. Linear interpolation functions are used for both types of elements. Values of $D_{ik}^{(l)}$ are equal to

$$D_{ik}^{(l)} = \sum_{k=1}^{3} \frac{B_iB_k + C_iC_k}{4\Delta^{(l)}} \tag{15}$$

and

$$D_{ik}^{(l)} = (-1)^{i+k}\frac{\pi}{2L^{(l)}} \tag{16}$$

for triangular element and rod-like element, respectively. $\Delta^{(l)}$ is the area of triangular element l, and $L^{(l)}$ is the length of the rod element. $B_1 = y_2 - y_3$ and $C_1 = x_3 - x_2$, where x and y are planar coordinates of the nodes in the triangular element. The other coefficients are obtained by cyclically permuting the subscripts. At the entrance, the net flows from all adjacent elements must satisfy the following relation:

$$\sum_{l'} q_i^{l'} = \frac{Q}{2} \tag{17}$$

where Q is the total volumetric flow rate of polymer melt. For the interior nodes, the net flows from all adjacent elements obey the conservation law of mass and are equal to zero, i.e.

$$\sum_{l'} q_i^{l'} = 0. \tag{18}$$

Equations (17) and (18) can be finally integrated and described by a matrix form of

$$[K]\{P\} = \{G\} \tag{19}$$

where $[K]$ is the element coefficient matrix, $\{P\}$ is the column matrix associated with pressure, P, and $\{G\}$ is the column matrix for variable, G_m. $G_m = Q/2$ if m represented in global node index number, is the entrance node of polymer melt. Otherwise, $G_m = 0$.

In solving equation (19), the boundary conditions at the melt front boundary, cavity side wall and melt inlet region must also be specified. At the melt-front nodes, the nodal pressures are equal to zero (gauge pressure), i.e.

$$P = 0. \tag{20}$$

Along the cavity side wall where the melt is impermeable, the boundary condition is specified as

$$\frac{\partial P}{\partial n} = 0. \tag{21}$$

In deriving equation (18) for nodes located on the cavity side, the melt flow rate across the cavity side wall is assumed to be zero, therefore, the boundary condition in the form of equation (21) is automatically fulfilled. Near the melt entrance region, the boundary conditions are specified according to the operating conditions of the melt and gas injection system. If the pressure is prescribed, then

$$P|_{\text{entrance}} = P_{\text{injection}} \tag{22}$$

and $P_{\text{injection}}$ is the injection pressure at the entrance. If volumetric flow rate is defined, then the boundary condition is expressed by

$$\oint_c \left(-S\frac{\partial P}{\partial n}\right) ds = Q/2 \tag{23}$$

where C is any closed contour lying in the melt-filled region and enclosing melt entrance. In the present paper, melt flow rate, Q, is determined from the filling speed during the melt injection period whereas, gas pressure is defined during the gas injection period. In

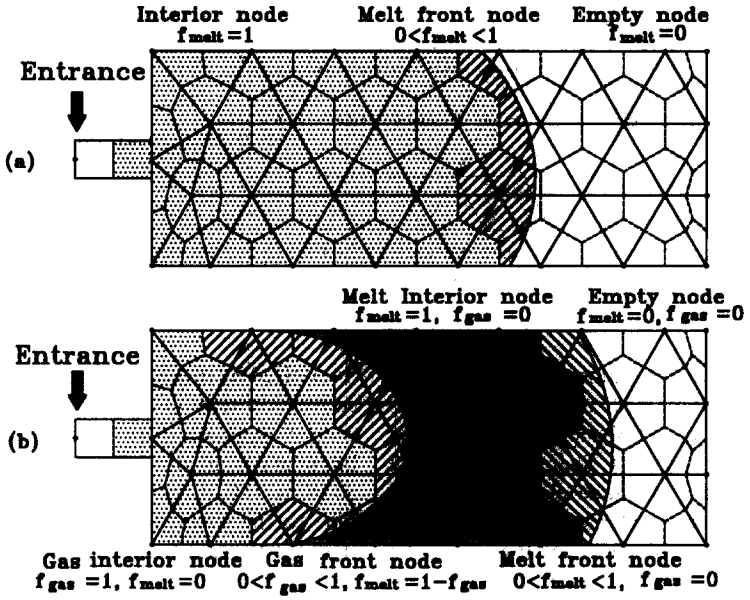

Fig. 4. (a) Schematic of the filling parameters used to identify the location of the melt front during melt injection. (b) Filling parameters used to identify the gas front nodes as well as gas interior nodes in the gas injection stage.

the former case, equation (23) is automatically satisfied when applying equation (17). To verify the numerical convergence in every analysis step, mass conservation at the melt entrance expressed by equation (17) is also checked once the pressure and flow rate $q_i^{(l)}$ in each sub-element are obtained. When gas pressure is prescribed during the gas injection period, the flow rate at the materials entrance is treated as unknown and variable rearrangement in the matrix described by equation (19) is required.

To distinguish the entrance node and the interior nodes from the melt-front nodes, a filling parameter f_{melt} is defined and calculated during all analyses. f_{melt} is equal to 1 for the entrance node and interior nodes, whereas $0 < f_{melt} < 1$ for melt-front nodes. When f_{melt} is 0, the node is designated as an empty node. A schematic of the node definition is shown in Fig. 4(a). At the melt-front nodes, the net flow entering the control volume from the neighboring elements which are filled with melt can be computed. Then the corresponding filling time required for filling the rest of the control volume of each melt front node can also be obtained. The analysis interval is chosen as the minimum of these filling times. By doing so, only one melt-front node gets filled per step. Once the pressure field is solved, the gapwise velocity profile and the associated shear rate values can be calculated. At the melt fronts, a uniform profile for temperature and gap-averaged velocity is assumed to count for the fountain flow effect. The numerical algorithm and procedure basically follow those reported [5–8].

In solving temperature field, the same method reported previously is used [5, 7]. The calculation of nodal temperature is basically weighted from the subvolumes of all adjacent elements. However, the convection term and the viscous-heating term consider only the contribution of the upstream elements. An implicit method is used for the conduction term, whereas the convection and viscous-heating terms were evaluated at the earlier step. Iteration criteria and algorithm are also similar to those in conventional injection molding [5, 7].

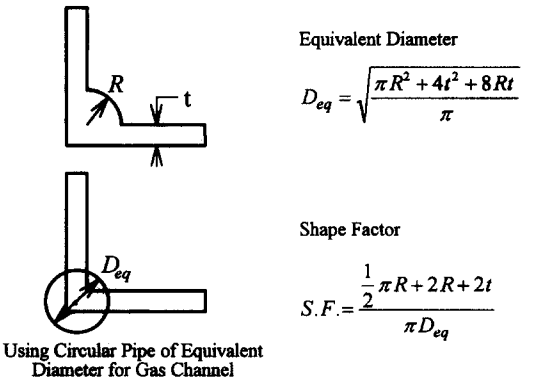

Fig. 5. A circular pipe of equal cross-section area is used to represent the gas channel with a cross-section of quarter circle and the connecting portion of the plate. The formulation of equivalent diameter as well as shape factor are also given.

Melt flow in a flow-leader type gas channel of non-circular cross-section. The geometry of the gas channel of quarter circular cross-section together with the connection portion in the thin part is approximated by a circular pipe of an equivalent hydraulic diameter D_{eq}. D_{eq} can be computed according to the description in Fig. 5 for the gas channel cross-section of a quadrantal shape. Also, the shape factor is defined and used to correct the excess heat transfer caused by the extra

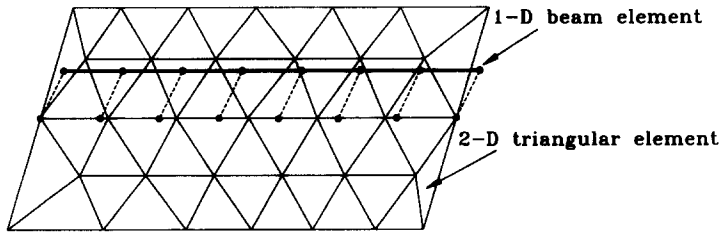

Fig. 6. Schematic diagram for the superimposition of the triangular shell element mesh and the two-node beam element mesh representing the thin part and gas channel, respectively.

area in using an equivalent diameter pipe. Once the shape factor value is obtained, it is combined with the thermal conductivity of polymer melt to take the excess heat transfer into account. Then the gas channel is modeled as a linear, two-node element which is superimposed on the part shell mesh of the triangular element. The situation is depicted in Fig. 6. In the simulation, a true volumetric flow rate is obtained from the real part volume. In solving the temperature field, the same method used for the regular, thin part is employed. However, the energy equation in the cylindrical coordinate system is used to solve temperature whenever the triangular part element node is superimposed on by the rod-like gas channel node. A verification of the present approach has been reported experimentally for melt front advancement within a rib-type flow leader of semicircular cross-section during conventional injection molding [8].

3.2. *Algorithm for gas and melt front advancements during gas injection*

Once the gas was injected into the mold either through a runner or cavity, the domain filled with gas is assumed to be of uniform pressure. The pressure at the gas injection node is assumed to be the injection gas pressure and the total flow rate of the melt is treated as unknown. Once the melt flow rate is solved, the gas front advancement around the gas injection node is determined by the melt flow rate in each sub-element of the control volume around this node. When the gas front advances, it is necessary to introduce a secondary filling parameter, f_{gas}, to identify the gas front nodes and gas interior nodes among the melt interior nodes filled with melt at previous instants, as specified in Fig. 4(b). The algorithm is similar to our particle-tracing algorithm, developed for both skin and core melt front advancements in the coinjection molding process reported recently [9]. Here, the injected gas was treated as core material with an additional assumption that the pressure be uniform within the gas region. However, for gas front nodes whose sub-elements contributed to the corresponding nodal control volume which involve both melt-filled elements and gas-filled elements, the mass conservation law must be derived based on the available volume for gas-filling by excluding those portions contributed to by coating melt. In solving temperature for the coating melt, a transient heat conduction equation discretized by the finite difference method is used. The convection term and the viscous-heating term in the energy equation can be neglected. A convective boundary is assumed at the gas/melt interface using 30 W m^{-2} $°C^{-1}$ for the heat transfer coefficient of gas. Due to the small time interval of the gas injection, the heat transfer from the coating melt to the gas is negligible.

4. EXPERIMENTS

A 75 ton Battenfeld 750/750 coinjection molding machine and airmold system were used for the present experiments. The melt temperatures for PS resin are 230 and 250°C and mold temperature are 40 and 60°C. A spiral tube part considered as the one-dimensional flow and a uniform thick hanger part of the two-dimensional planar flow condition were first gas injection molded to provide experimental verification for the present simulation scheme. Then a thin part of the angle bracket shape designed with a gas channel in a quadrantal cross-section geometry was also gas injection molded. In all cases, the coating melt thickness along the gas flow direction was measured. Detailed experimental procedures are described elsewhere [11].

For polystyrene (CHI MEI/PG33), materials constants in the modified-Cross model used for the viscosity values are $n = 0.2838$, $\tau^* = 1.791 \times 10^4$ Pa, $B = 2.591 \times 10^7$ Pa·s and $T_b = 11\,680$ K. Density, specific heat and thermal conductivity of PS are 940 kg m^{-3}, 2100 J $kg^{-1} \cdot K^{-1}$ and 0.18 W $m^{-1} \cdot K^{-1}$, respectively.

5. RESULTS AND DISCUSSIONS

5.1. *Case of straight circular tube (numerical test for convergence)*

In order to verify the convergence of the present numerical algorithm, a straight circular tube of 20 cm long filled with 70% Newtonian fluid under an isothermal condition, followed by an injection of gas at 100 bar pressure was assumed for a test. Assuming a 25% coating melt thickness ratio, the theoretical gas penetration length is expected to be 10.67 cm long under an incompressible assumption for melt. The simulated result is 10.5 cm. Numerical accuracy is within 2%.

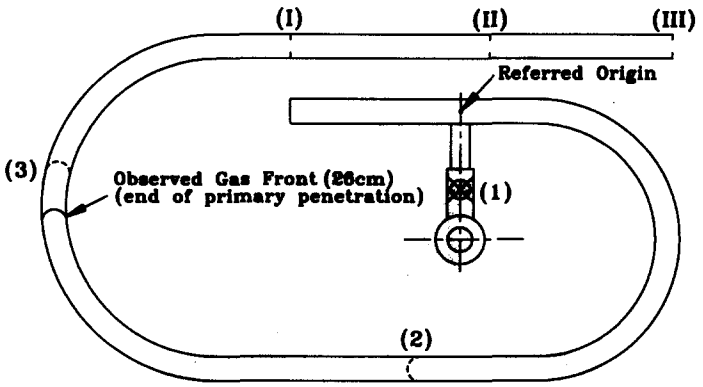

Fig. 7. Predicted and experimental results of the gas front locations in a gas-assisted injection molded spiral tube.

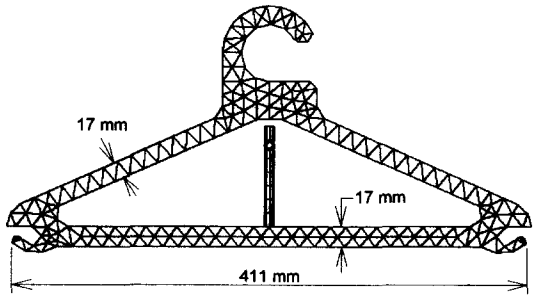

Fig. 8. Geometry and finite element mesh of a hanger part of uniform thickness.

5.2. *The case of the spiral part (one-dimensional flow)*

The second test example is a spiral tube. The spiral tube is a gas-assisted injection molded and the distribution of coating melt thickness was carefully measured along gas penetration path [11]. The coating melt thickness friction measured from experiments was about 0.36. Using this layer ratio, simulated results for the prediction of gas front advancement is shown in Fig. 7. Experimental observation of the gas front location is also indicated. The simulated result shows reasonably good consistency with experimental observation, although the secondary gas penetration occurring in the post-filling phase as a result of melt shrinkage was not included at the present time. The result is also consistent with the theoretical value calculated from the injected volume of gas.

5.3. *Case of uniform thick hanger part (two-dimensional planar flow)*

The experimental mold (Fig. 8) is a hanger part with 7 mm uniform thickness. Both gas and melt are injected from nozzle. After 82% of melt injection, gas of 70 bar pressure was injected. Gas penetration within the part is shown in Fig. 9. The uniform, thick hanger mold can be considered as a two-dimensional planar flow for both gas and melt. The measured melt layer ratio was about 0.37. The filling time under full polymer injection shot is 1.46 s and gas is injected at 82% melt injection stroke. Simulated gas penetration, represented by skin thickness ratio, is shown in Fig. 10. The predicted locations for the final gas fronts, although slightly ahead, are reasonably good as compared with those found from experiment. The observed gas front located on the top of the part is in good coincidence with the predicted location. In principle, the second gas penetration (the shorter one) should occur on the right hand portion of hanger handle. This is because the rectangular region below the hanger hook results in a slightly larger flow resistance than that of the left hand flow path. Gas is expected to flow easier on the left side. However, the shorter gas penetration actually occurred on the left handle because of the gravitation effect resulting from mold set-up (cavity of left handle locates on the bottom of the mold) during the experiments. Despite that, the second gas fronts (for observed and predicted, respectively) penetrate at different sides of hanger handle, the observed length and the predicted length for this shorter gas penetration were quite close. The present simulation is also positively confirmed by the experiments.

5.4. *Case of thin, angle bracket plate with gas channel of quadrantal cross-section (mixed characteristics of one-dimensional and two-dimensional flow)*

The geometry and the associated mesh for the thin, angle bracket part (thickness 1.56 mm) designed with a rib-type gas channel of quadrantal cross-section (of a radius 5.4 mm) is shown in Fig. 11. This part geometry represents the one-dimensional and two-dimensional flow characteristics for both melt and gas. The gas injection molded part with gas penetration can be seen in Fig. 12. Based on the formula

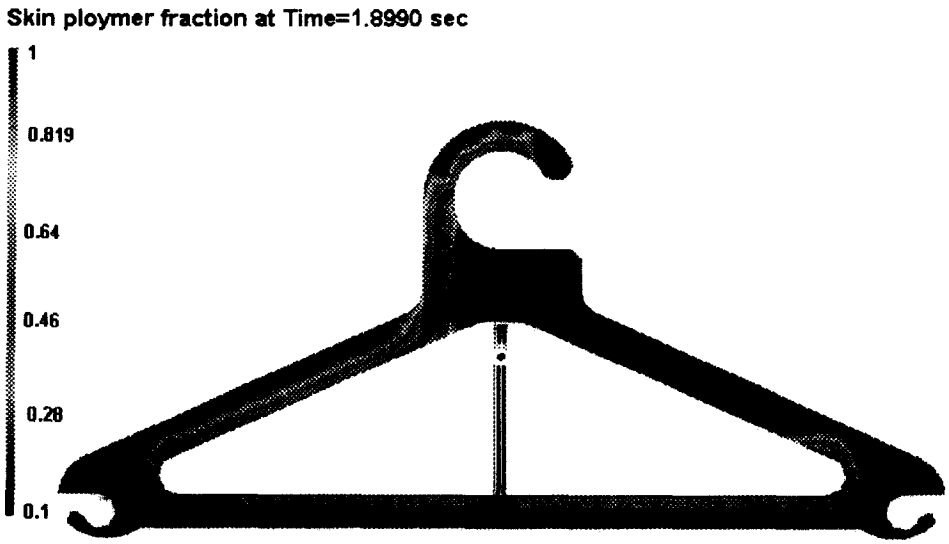

Fig. 10. Simulated result of gas penetration at the end of the filling process in a molding hanger part.

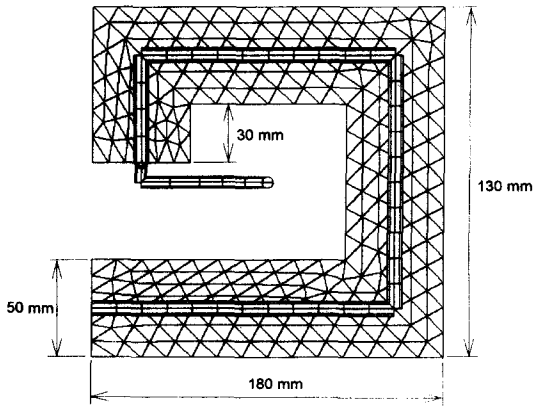

Fig. 11. Geometry and finite element mesh of the angle bracket part laid out with the gas channel.

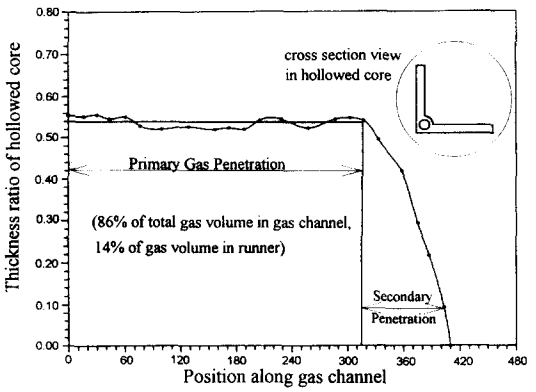

Fig. 13. Distribution of thickness ratio for the hollowed core along the gas channel. The associated view of the cored-out cross-section by gas is also depicted.

given in Fig. 5, the calculated equivalent diameter D_{eq} for the quadrantal gas channel was 7.33 mm and the value of the shape factor is 0.97. Analyzed conditions are 0.9 s filling time for full shot and gas injection at 93% melt injection stroke (corresponding to 0.837 s of melt injection). The injected gas pressure was 130 bar. The distribution of the skin melt thickness along the gas channel and the corresponding view of the cored out cross-section are depicted in Fig. 13. From the area of the cored out section and the total area of cross-section (or the area enclosed by the tube of equivalent diameter), the estimated ratio for the hollowed core thickness was about 0.537. The calculated melt shrinkage from the pressure-volume-temperature (P-V-T) equation of state is 8% corresponding to a 94 mm length for the secondary gas penetration. The estimated length for the secondary phase of gas penetration is consistent with that found from the variation profile of the hollowed core thickness ratio, as indicated in Fig. 12. The simulated results for both gas and melt front advancements after 0.406 s of gas injection and at the end of filling stage are shown in Fig. 14(a and b), respectively. Again, the predicted result of the final gas front location is also in good coincidence with the observed location.

6. CONCLUSION

A numerical algorithm based on the control-volume/finite-element method combined with particle tracing scheme was developed to simulate gas and melt front advancement during the gas-assisted injection molding process. Melt and gas flow in the gas channel of quadrantal cross section were approximated by a flow model which superimposes a circular pipe of equivalent diameter on the thin plate. The simulated results are also compared with experimental observation. All the verification of the simulations in one-dimensional, two-dimensional and a mixed one- and two-dimensional conditions by the experiments are positive. Although the effects of the processing condition on the coating layer ratio remain to be inves-

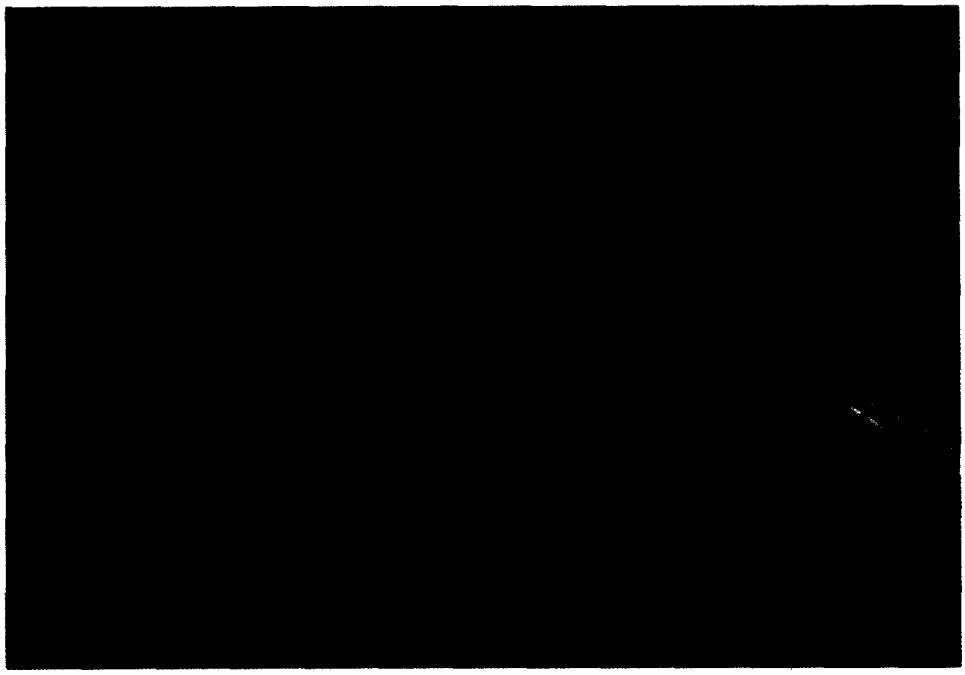

Fig. 9. Experimental result of gas penetration in the gas-assisted injection molded hanger.

Fig. 12. Experimental result of the gas-assisted injection molded part.

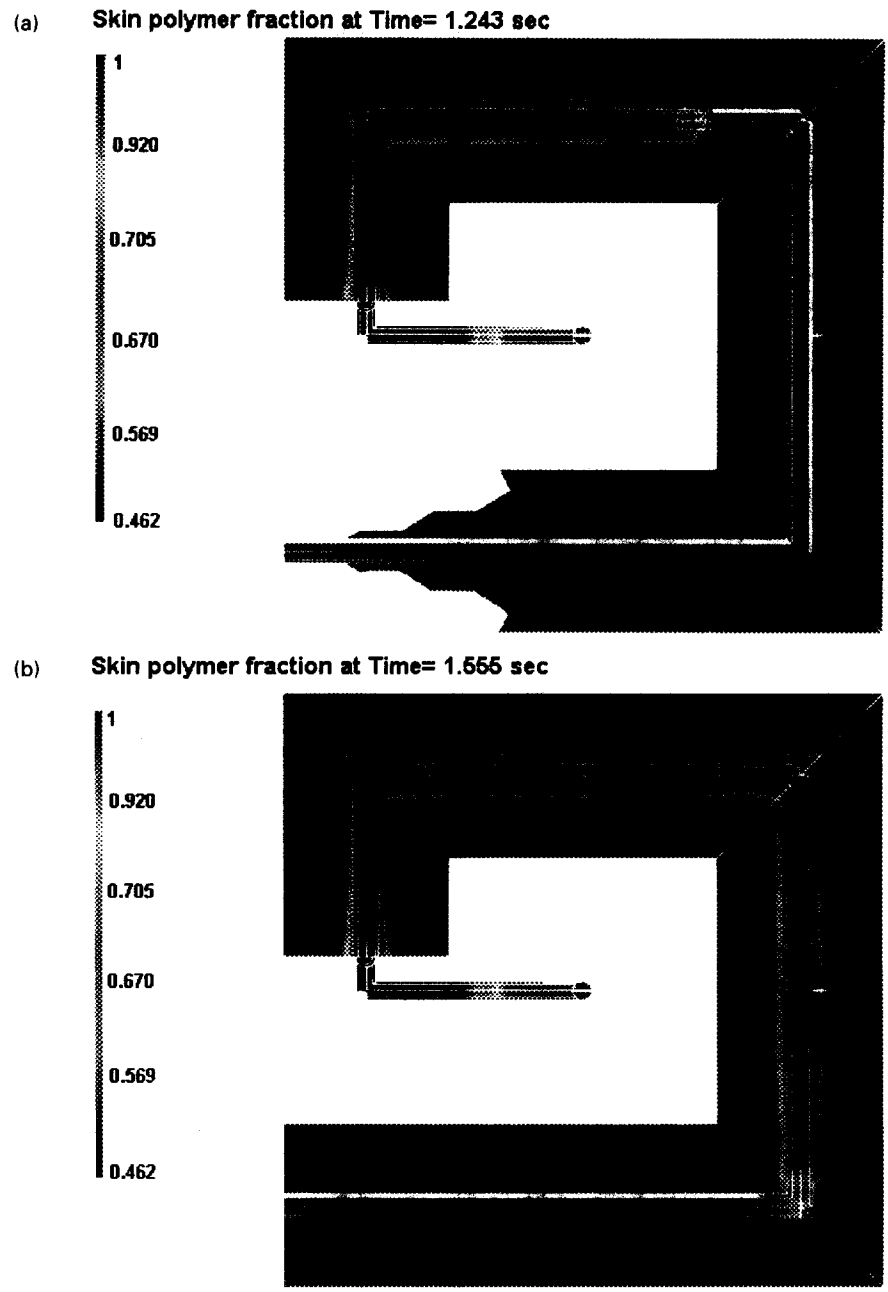

Fig. 14. (a) Simulated result of gas front location after 0.406 s of gas injection. (b) Simulated result of gas penetration at the end of the gas-assisted injection molding.

tigated to establish a general empirical formula, the current numerical scheme provides reasonably good results in the prediction of gas penetration in gas-assisted injection molding.

Acknowledgements—This work was supported by National Science Council under NSC grant 83-0405-E033-071.

REFERENCES

1. K. C. Rush, Gas-assisted injection molding—a new technology is commercialized, *Plastics Engnrs* July, 35–38 (1989).
2. S. Shah, Gas injection molding: current practices, *SPE Tech. Papers* **37**, 1494–1506 (1991).
3. L. S. Turng, Computer-aided engineering for the gas-assisted injection molding process, *SPE Tech. Papers* **38**, 452–456 (1992).
4. S. Shah and D. Hlavaty, Gas injection molding: structural application, *SPE Tech. Papers* **37**, 1479–1493 (1991).
5. V. W. Wang, C. A. Hieber and K. K. Wang, Dynamic simulation and graphics for the injection molding of three-dimensional thin parts, *J. Polym. Engng* **7**, 21–45 (1986).
6. A. Davidoff, S. C. Chen and H. Bung, PROCOP: a stress and flow analysis package for injection molding, *SPE Tech. Papers* **36**, 393–396 (1990).
7. S. C. Chen, P. Pai and C. Hsu, A study of finite element mold filling analysis in applications, *Ann. Tech. Paper SPE* **34**, 250–254 (1988).

8. S. C. Chen and K. F. Hsu, Simulation of the melt front advancement in injection molded plate with a rib of semicircular cross-section, *Numer. Heat Transfer A* **28,** 121–129 (1995).
9. S. C. Chen and K. F. Hsu, Numerical simulation and experimental verification of melt front advancements in coinjection molding process, *Numer. Heat Transfer A* **28,** 503–513 (1995).
10. K. H. Huebner and E. A. Thornton, *The Finite Element Method for Engineers*, Chaps 4 and 5. Wiley, New York (1982).
11. S. C. Chen, M. C. Jeng, K. S. Hsu and K. F. Hsu, Study of gas-assisted injection molding process and its computer integrated manufacturing technology, Progress Report of NSC, (1994).